Biomolecules and Biomedicine
ISSN: 2831-0896 (Print) | ISSN: 2831-090X (Online)
Journal Impact Factor® (2024): 2.2
CiteScore® (2024): 5.2
www.biomolbiomed.com | blog.bjbms.org

RESEARCH ARTICLE

Osmanović et al: Marine hits for H_2 and proton pump

Virtual screening of marine coumarins and xanthenes identifies novel acid-suppressive leads targeting histamine H_2 receptor and gastric proton pump

Amar Osmanović[1], Mirsada Salihović[1*], Amila Mehmedović[2,3], Amila Turalić[1], Elma Veljović[1], Mirha Pazalja[1], Simone Carradori[4], Selma Špirtović-Halilović[1]

[1]University of Sarajevo, Faculty of Pharmacy, Sarajevo, Bosnia and Herzegovina;

[2]Gastroenterohepatology Clinic, Clinical Center of University of Sarajevo, Sarajevo, Bosnia and Herzegovina;

[3]University of Sarajevo, Faculty of Health Studies, Sarajevo, Bosnia and Herzegovina;

[4]Department of Pharmacy, "G.d'Annunzio" University of Chieti-Pescara, Chieti, Italy.

*Correspondence to Mirsada Salihović: mirsada.salihovic@ffsa.unsa.ba

DOI: https://doi.org/10.17305/bb.2026.13660

ABSTRACT

Marine natural products represent a diverse collection of structurally distinct metabolites, many of which have untapped therapeutic potential. This study screened 161 marine-derived coumarin and xanthene compounds for their binding affinity to the histamine H_2 receptor and the gastric H^+/K^+-ATPase, the primary regulators of gastric acid secretion. Docking simulations were performed using curated structures of both targets, followed by an evaluation of the compounds for drug-likeness and predicted absorption, distribution, metabolism, and excretion (ADME) properties. Thirty-four compounds demonstrated a stronger predicted affinity for the H_2 receptor than famotidine; however, only three compounds (1, 5, and 150) met all drug-likeness criteria, achieving quantitative estimates of drug-likeness (QED) values exceeding 0.67. Screening against the proton pump yielded 98 hits with higher affinity than soraprazan, with compound 150 being the only candidate to fulfill all medicinal chemistry filters. Interaction analysis indicated that compound 150 binds to the proton pump in a manner that largely overlaps with soraprazan. Density functional theory (DFT) calculations were utilized to characterize the electronic properties of the most promising compounds. ADME predictions suggested favorable permeability and a low risk for human ether-à-go-go-related gene (hERG) inhibition, although high plasma protein binding and the potential for cytochrome P450 (CYP) inhibition may require further optimization. These findings underscore the potential of pyranocoumarin compound 150, along with xanthene derivatives 1 and 5, as promising candidates for the development of new acid-suppressive agents.

Keywords: Marine compounds, coumarin, xanthene, histamine H_2 receptor, gastric H^+/K^+-ATPase, virtual screening.

INTRODUCTION

Normal gastric acid secretion is necessary for digestion and for protecting the stomach from pathogens. However, when acid production becomes excessive or dysregulated, it contributes to several common gastrointestinal disorders. Common causes of hypersecretion include *Helicobacter pylori* infection, gastrin-secreting tumors in Zollinger–Ellison syndrome, antral G-cell hyperplasia, which act through different mechanisms to overstimulate gastric parietal cell [1]. Persistent acid overproduction is central to the pathogenesis of gastroesophageal reflux disease (GERD) and peptic ulcer disease and may eventually drive Barrett's esophagus and esophageal adenocarcinoma [2]. What we eat can also really shape how our stomach handles acid. For example, meals that are high in protein, as well as certain drinks like milk or fermented beverages, tend to boost acid production. On the other hand, foods that are heavy or high in fat usually slow down how quickly the stomach empties. That slower emptying keeps gastrin levels up for longer, which means the stomach continues releasing more acid. In some individuals, strongly seasoned foods may additionally irritate the mucosa and provoke further stimulation [3,4].

Management of acid-related disorders generally relies on approaches that either reduce the production of acid or neutralize acid already present in the stomach. Neutralization is achieved with antacids, which include inorganic salts such as sodium bicarbonate, magnesium hydroxide, and calcium carbonate, as well as bismuth or aluminum-containing compounds like silicates. These agents work by buffering or adsorbing excess gastric acid. In contrast, acid-suppressive therapy uses drugs that interfere with acid secretion, most notably histamine H_2 receptor antagonists (H_2RAs) and proton pump inhibitors (PPIs) [2,5].

H_2RAs reduce gastric acid by blocking histamine from binding to H_2 receptors on parietal cells. This lowers both resting acid output and the surge that follows meals. Famotidine is still used quite often, although its benefit can taper off with prolonged therapy because patients develop tachyphylaxis [6,7]. Ranitidine was once widely prescribed as well, but it has largely disappeared from clinical use after multiple formulations were found to contain *N*-nitrosodimethylamine (NDMA), a compound classified as probably carcinogenic to humans [8].

PPIs, such as omeprazole, lansoprazole, and pantoprazole, provide stronger, longer-lasting acid suppression by irreversibly blocking the gastric H^+/K^+-ATPase. They're generally very effective, but they are associated with certain drawbacks. They tend to work more slowly, their effects can vary from person to person, and long-term use has raised concerns about potential risks, including *C. difficile* infections, chronic kidney issues, and certain nutrient deficiencies [9–12]. Practical issues also come up, since taking PPIs with food can delay their absorption and reduce bioavailability, and H_2RAs often need some planning around meals or known triggers [13].

A newer group of medications, potassium-competitive acid blockers (P-CABs) such as soraprazan, vonoprazan, and tegoprazan, offers another option. These drugs inhibit the proton pump by competing at the potassium-binding site and, in general, produce quicker and more consistent acid suppression than older therapies [9,10,14]. Despite their widespread use, these drugs have several well-recognized limitations, long-term safety profiles are still being established, so new therapeutic approaches remain worth exploring.

Coumarins and xanthenes have been extensively studied for decades as natural-product scaffolds, and their core structures continue to make them appealing starting points in drug discovery. The characteristic benzopyrone and dibenzo-γ-pyrone ring systems give these molecules relatively rigid, planar shapes, with carbonyl and phenolic oxygen atoms arranged in ways that meaningfully affect their polarity, hydrogen-bonding behavior, and overall lipophilicity. These features help account for the broad spectrum of biological activities reported for both classes and explain why they fall into a part of chemical space frequently associated with drug-like compounds. For this reason, coumarins and xanthenes are frequently regarded as "privileged" scaffolds and are commonly used as starting points in early lead discovery and optimization efforts [15–18].

Marine-derived metabolites extend this diversity even further. Organisms from marine environments (mostly fungi and bacteria) produce numerous coumarin and xanthene derivatives, many of which have shown antimicrobial, anti-inflammatory, or anticancer properties [19]. Secondary metabolites (coumarins and xanthenes) are typically isolated by fermentation of the producing fungus/bacterium followed by ethyl acetate extraction of the culture broth and biomass, and subsequent

chromatographic purification to yield the target compounds [20–22]. The range of biological activities suggests that marine-derived compounds from these structural families may represent promising candidates for further investigation. Xanthenes (more precisely their close structural relatives, xanthones) are frequently implicated in antisecretory or cytoprotective pathways [23–26]. Although studies specifically examining marine-derived coumarins and xanthenes in gastric acid suppression are scarce, work on plant-derived analogues provides some useful context. Several coumarins of terrestrial origin have been reported to inhibit the gastric H^+/K^+-ATPase, with IC_{50} values ranging from approximately 110 to 638 µM. Xanthenes have shown similar activity *in vitro*, with IC_{50} values ranging between 47 µM and 1.6 mM, which points to their potential as acid-suppressive compounds [27]. In addition, various coumarin derivatives exhibit gastroprotective properties, including urease inhibition against *Helicobacter pylori* and measurable anti-ulcer effects [28]. These observations suggest that marine-derived coumarin and xanthene structures could be worth examining further in the context of gastric acid–related conditions.

Computational methods have taken on an increasingly central role in early-stage drug discovery. Molecular docking is now routinely used to explore how candidate ligands might interact with their intended targets and to estimate their binding affinities. At the same time, assessments of drug-likeness, drawing on criteria such as Lipinski's, Veber's, and Egan's rules, as well as metrics like the quantitative estimate of drug-likeness (QED), offer a practical way to assess the pharmacokinetic and overall development potential of new compounds [29–32]. In addition, density functional theory (DFT) calculations are often employed to examine the electronic properties of the investigated drug-like candidates, useful for complementing interpretation of ligand–target interactions. *In silico* screening of marine-derived coumarin and xanthene derivatives against both the histamine H_2 receptor and the gastric proton pump therefore represents a rational strategy to identify candidates that may overcome the limitations of existing therapies.

MATERIALS AND METHODS

Virtual screening

In total 161 compounds focusing on xanthene and coumarin scaffolds isolated from marine organisms [20–22,33–58] were selected for *in silico* screening. These

derivatives were identified through a systematic literature search aimed at maximizing structural diversity within these classes. During the selection process, we deliberately excluded any compounds with previously reported cytotoxicity or established toxicological liabilities (e.g. aflatoxins) to prioritize those with the greatest potential for therapeutic safety. Along with these, the reference ligands famotidine, a histamine H_2 receptor antagonist, and soraprazan, a potassium-competitive acid blocker were added to the library. Ligand 3D conformations were generated from SMILES strings and prepared using the AutoSMILES protocol in YASARA Structure v23.9.29 [59,60]. To ensure accurate docking precursors, protonation states were assigned based on a physiological pH of 7.4 by predicting pK_a values and optimizing the hydrogen-bonding network through the experiment neutralization procedure. This protocol identified the most energetically favorable tautomeric states at the specified pH while strictly maintaining the stereochemistry defined in the input SMILES. Final structural refinement was performed *via* energy minimization using the AMBER14 force field [61], which optimized bond lengths and angles to a local energy minimum without altering predefined chiral centers.

The histamine H_2 receptor (PDB ID: 7UL3) and the gastric H^+/K^+-ATPase (PDB ID: 7W49) were retrieved from the Protein Data Bank (PDB). Target protein structures were prepared by removing all crystallographic water molecules while retaining all other heteroatoms, including structural ions and cofactors, to preserve the native protein fold and structural stability. Polar hydrogen atoms were added, and protonation states were assigned for a physiological pH of 7.4 using YASARA's automated pK_a prediction and experiment neutralization protocols. Final structural refinement was performed through energy minimization using the AMBER14 force field to resolve steric clashes and optimize the geometry of the target prior to docking. The stereochemical quality of the refined models was validated using the MolProbity web server [62], with backbone dihedral distributions evaluated based on high-accuracy Ramachandran criteria [63]. Corresponding plots and residue statistics are provided in the Supplemental Material (Figures S1 for histamine H_2 receptor and S2 for gastric proton pump).

Docking simulations were performed with AutoDock [64], as implemented in YASARA Structure. The docking grid was positioned to encompass the established binding pockets, using the locations of the co-crystallized ligands as a guide. The grid box was centered at (x, y, z) = (-7.619, 8.752, 11.276) Å with dimensions of (15.24 ×

17.50 × 22.55) Å within the chain A (7-transmembrane helices) for H_2 receptor, and centered at (x, y, z) = (-10.811, 9.935, 9.245) Å with dimensions of (21.62 × 19.87 × 18.49) Å within the chain A (potassium-transporting ATPase alpha chain 1) for proton pump. The Lamarckian genetic algorithm was applied with the following settings: per each ligand 25 docking runs were performed, a maximum of 5 000 000 energy evaluations, 27 000 generations per run, and a grid point spacing of 0.375 Å, ensuring the identification of the lowest-energy docked poses. Docking simulations were performed using a rigid receptor model with flexible ligand sampling. For each ligand, multiple poses were generated and automatically clustered by YASARA based on structural similarity to identify representative binding modes. The best-ranked poses for each ligand were selected for interaction analysis based on predicted binding energy and cluster population. To check that the docking setup was performing reliably, we redocked the original co-crystallized ligands; RMSD values of 1.3532 Å for famotidine and 1.5003 Å for soraprazan (Supplemental Figure S3) were taken as evidence that the protocol was reproducing the experimental binding modes accurately. Docking results were reported as binding energy (ΔG, kcal/mol), predicted dissociation constants (Kd, μM), and ligand efficiency values (ΔG per heavy atom).

Calculation of drug-likeness and physicochemical parameters

Drug-likeness and physicochemical parameters were calculated with RDKit [65]. The evaluation included Lipinski's Rule of Five (molecular weight (MW), logP, hydrogen bond donors (HBD) and acceptors (HBA)), Veber's rules (topological polar surface area (TPSA) and rotatable bond (RotB) count), and Egan's filter (logP, TPSA), together with the quantitative estimate of drug-likeness (QED) [32]. QED score integrates descriptors such as lipophilicity, molecular weight, hydrogen bonding capacity, aromaticity, and structural alerts into a single metric. Scores above 0.67 were taken as indicative of compounds with generally favorable drug-like profiles. Additional descriptors such as fraction of sp^3 carbons, aromatic ring count, and other physicochemical measures were also considered.

Density functional theory calculations

Density functional theory (DFT) calculations were performed to investigate the electronic properties of the selected coumarin and xanthene derivatives. All calculations were carried out using the Spartan 14 software [66]. Geometry

optimizations were conducted using the B3LYP functional in combination with the 6-31G(d) basis set, without any symmetry constraints. The optimized structures were confirmed as true minima on the potential energy surface by the absence of imaginary frequencies.

Frontier molecular orbitals (HOMO and LUMO) were calculated for the optimized geometries, and the HOMO–LUMO energy gap was used as an indicator of molecular reactivity. Global reactivity descriptors, including chemical potential (μ), global hardness (η), softness (S), and electrophilicity index (ω), were estimated from HOMO and LUMO energies as described by Parr et al. [67]. In addition, dipole moments were calculated for the optimized geometries to characterize the overall molecular polarity of the investigated compounds.

Prediction of ADMET parameters

Pharmacokinetic and toxicological properties of the marine-derived compounds were evaluated using the ADMETlab 2.0 online platform [68]. The tool predicts key absorption, distribution, metabolism, excretion, and toxicity (ADMET) parameters through multiple machine learning models trained on experimental datasets. For each compound, parameters such as intestinal absorption (HIA), Caco-2 permeability, plasma protein binding (PPB), blood–brain barrier (BBB) penetration, P-glycoprotein substrate/inhibitor status, major cytochrome P450 (CYP) inhibition potential, and toxicological alerts were computed. The resulting numerical outputs were categorized as favorable, moderate, or risk according to ADMETlab's internal thresholds, and used to rank compounds for further analysis.

Statistical filtering and comparisons were carried out in Python v3.10 using the pandas library, while docking poses, 2D interaction diagrams, and protein–ligand complex visualizations were prepared with Discovery Studio Visualizer v24.1.0.23298.

RESULTS

Molecular docking study of the 161 tested compounds against the H_2 receptor and gastric H^+/K^+-ATPase revealed a broad distribution of binding affinities, dissociation constants (Kd), and ligand efficiencies (Figure 1).

Binding energies (ΔG) obtained from docking provide a measure of ligand–receptor interaction strength, where more negative values correspond to stronger and more favorable binding affinities [64]. From these values, estimated dissociation constants (Kd) can be derived, representing the concentration of ligand at which half of the receptor sites are occupied; lower Kd values therefore indicate stronger binding [69]. Beyond binding affinity, the predicted ligand efficiency provides an indication whether a ligand is likely to induce a notable biological effect once bound. This distinction is useful for separating compounds that bind strongly but are unlikely to be active from those that may exhibit meaningful pharmacological activity [70]. Taken together, these parameters helped us to prioritize compounds that combined strong binding with plausible functional relevance.

Famotidine was selected as the H_2 receptor reference ligand owing to its clinical relevance and availability of a cryo-EM structure (PDB ID 7UL3) [71]. Soraprazan was selected as the gastric H^+/K^+-ATPase reference ligand, and the reason behind choosing soraprazan instead of some PPI was that unlike PPIs that require acid activation and form irreversible covalent bonds, it is a P-CAB that reversibly inhibits the H^+/K^+-ATPase at the K^+-binding site [72,73]. High-resolution structural data for P-CABs, including the soraprazan–pump complex (PDB ID: 7W49), enabled accurate docking and binding-energy comparison [72]. In contrast, PPIs lack resolved crystal structures with the proton pump due to their transient, pH-dependent activation and covalent binding [73].

When benchmarked against the reference antagonist famotidine (binding energy −7.22 kcal/mol, Kd 5.10 μM, efficiency 0.361 kcal/mol*Atom), 34 compounds demonstrated superior binding energy and Kd (Supplemental Excel File, sheet 1). Docking against the gastric proton pump showed an even higher proportion of favorable interactions. Relative to the reference drug soraprazan (binding energy −7.95 kcal/mol, Kd 1.49 μM, efficiency 0.294 kcal/mol*Atom), 98 ligands achieved superior binding energies and dissociation constants (Supplemental Excel File, sheet 2), suggesting that members of the library are capable of binding favorably to the proton-pump pocket.

Drug-likeness was evaluated using the Quantitative Estimate of Drug-likeness (QED), which combines several physicochemical descriptors into a single score between 0

and 1. Higher values reflect properties commonly seen in approved small-molecule drugs. In practice, compounds with QED values above approximately 0.67 are generally considered to have favorable drug development potential. This metric was used alongside the traditional filters of Lipinski (MW ≤ 500, logP ≤ 5, HBD ≤ 5, HBA ≤ 10), Veber (TPSA ≤ 140 Å^2, RotB ≤ 10), and Egan (logP ≤ 5.88, TPSA ≤ 131.6 Å^2), which evaluate factors such as molecular weight, lipophilicity, hydrogen-bonding capacity, flexibility, and polar surface area. Lastly, the three compounds have zero alerts for the Pan-Assay Interference Compounds (PAINS) substructures. This indicates that their chemical scaffolds do not contain the reactive moieties (such as quinones, catechols, or ene-rhodanines) typically linked to promiscuous protein binding or redox cycling in assay conditions. Together, these criteria help identify molecules with a balanced physicochemical profile and a reasonable likelihood of good pharmacokinetic properties [32].

Integration with drug-likeness profiles revealed that only a subset of the previously filtered strong binders complied with multiple medicinal chemistry filters. Specifically, from 34 marine compounds being better than famotidine in binding affinity against H_2 receptor, only three fulfilled Lipinski's rule of five, Veber, and Egan criteria while maintaining QED > 0.67 (Table 1, columns 2, 3 and 4). These compounds represent the most promising follow-up candidates for H_2 receptor modulation, combining favorable docking scores with drug-like properties. The high rate of QED > 0.67 in this set of compounds further suggests balanced complexity and tractability. Structures of these three compounds are shown in Figure 2.

Drug-likeness filtering of 98 marine compounds being better than soraprazan in binding affinity against proton pump, narrowed the cohort to only one compound that satisfied Lipinski, Veber, and Egan criteria while maintaining QED > 0.67 (Table 1, column 5).

Chemical space analysis of the selected ligands indicated that all compounds were positioned within the classical drug-like region defined by Lipinski, Veber, and Egan criteria, with QED values in the favorable range (≥ 0.67). Most of the screened coumarin and xanthene derivatives clustered within a similar range of molecular weight, polarity, and lipophilicity (Supplemental Excel File, sheet 3). These values fall within the range typically observed for many GPCR-active small molecules.

When compared to the reference ligands, the marine candidates showed greater aromaticity and rigidity than famotidine, but lower bulk and polarity than soraprazan, implying that these compounds may achieve reasonable permeability while still effectively engaging the receptors.

To complement the docking results with an electronic-structure perspective, quantum-chemical descriptors were calculated for the three prioritized candidates (compounds **1**, **5**, and **150**) at the B3LYP/6-31G(d) level. The HOMO–LUMO gap (ΔE) and conceptual DFT descriptors (μ, η, S, and ω), together with the dipole moment, were used to characterize molecular stability/polarizability and overall polarity, which can influence electrostatic and hydrogen-bonding contributions to ligand–target interactions (Table 2).

Figures 3 and 4 show the main interactions formed by the selected compounds with their respective targets. In the case of the H_2 receptor, the binding patterns differ considerably from those of famotidine, which is not surprising given the structural differences between the molecules. Compounds **1** and **5**, both belonging to the xanthene class, exhibit similar interaction profiles with the H_2 receptor (interacting with Tyr94, Tyr78 and Leu274), however showing only a single interaction as famotidine, with Asp98 and Tyr278, respectively. In contrast, compound **150**, based on a pyranocoumarin scaffold, engages the H_2 receptor through a distinct set of interactions, overlapping with famotidine at Asp98 and Cys102 (Figure 3).

On the other hand, compound **150** shows a high degree of overlap in its interaction pattern when compared to soraprazan, screened against the gastric proton pump; eight of the nine key contacts observed for the candidate are also present in soraprazan's binding mode (Figure 4).

After applying the drug-likeness filters and QED thresholds, the remaining compounds were subjected to ADME analysis to evaluate their pharmacokinetic suitability (Table 3). The assessment focused on properties important for oral absorption and systemic distribution, including Caco-2 permeability, human intestinal absorption (HIA), plasma protein binding (PPB), and predicted blood–brain barrier (BBB) penetration. Interactions with key transporters and metabolic enzymes, such as P-glycoprotein (P-gp) and CYP3A4 or CYP2D6, were also examined. We additionally checked the likelihood of hERG channel inhibition to estimate potential

cardiotoxicity. Together, these parameters provided an overview of each compound's absorption, metabolism, and overall safety profile, helping to identify the most promising candidates. Only a subset of the ADMETlab outputs is reported here; full results are available in the Supplemental Material (Supplemental Excel File, sheet 6). These parameters provided an integrated view of the pharmacokinetic properties and potential safety liabilities of the prioritized compounds, further supporting the selection of candidates with the most favorable absorption and metabolic profiles.

DISCUSSION

When comparing results across the two targets, a clear difference in hit distributions becomes apparent. The H_2 receptor screen yielded fewer high-confidence ligands, but the best three candidates demonstrated strong compliance with drug-likeness rules, making them more directly translatable to medicinal chemistry follow-up. In contrast, the proton pump assay produced a much larger pool of raw docking outperformers, but all except one fell short in terms of QED or rule compliance. This indicates that while the chemical library is rich in structural motifs capable of engaging the proton pump binding site, optimization for drug-likeness is necessary to progress these scaffolds. While docking is useful for narrowing down candidates, some high-scoring molecules still lack properties needed for further development. For the H_2 receptor, a focused shortlist of three compounds can be prioritized for synthesis and biological validation. For the proton pump, although 98 ligands initially outperformed soraprazan *in silico*, a stricter filtering leaves only one, but highly promising, candidate for follow-up.

Leptosphaerolide (compound **150**) is described as a novel, degraded polyketidic lactone isolated from *Leptosphaeria orae-maris* [34]. The fungus *L. orae-maris* is recognised in marine natural-products research as a source of secondary metabolites [74]. There is no well-documented *in silico*/ADMET prediction for leptosphaerolide in the literature. Due to the limited data on its pharmacology or ADMET profile, leptosphaerolide represents a novel scaffold, less characterised than other candidates, and any *in silico* results should be considered exploratory.

Leptosphaerolide emerged as a dual candidate, exhibiting favorable profiles against both targets. It could provide a basis for exploring therapies that simultaneously modulate both pathways. A compound capable of influencing both the H_2 receptor

and the proton pump could be particularly useful for patients who continue to experience symptoms despite standard single-target therapies.

Penicixanthene B (compound **5**) was isolated from the mangrove-derived fungus *Penicillium sp*. JY246 that was obtained from the stem of *Ceriops tagal*. It showed insecticidal activity against larvae of *Helicoverpa armigera* and *Culex quinquefasciatus* [20]. A newer derivative, Penicixanthene E (compound **1**), from the same fungal genus showed weak cytotoxic activity against the human pancreatic cancer cell line SW1990 [21]. The pharmacological activity and ADMET characteristics of penicixanthenes in humans have not been investigated, so these molecules remain largely uncharacterized and warrant further biological studies.

Since no published studies have investigated marine-derived coumarins or xanthenes as inhibitors of the gastric H^+/K^+-ATPase or as histamine H_2-receptor antagonists, the interpretation of our *in silico* results rely on the closest relevant evidence from terrestrial plant–derived analogues. Reyes-Chilpa et al. reported that several naturally occurring xanthones inhibit the gastric H^+/K^+-ATPase, with IC_{50} values ranging from approximately 47 μM to 1.6 mM, reflecting moderate but structure-dependent potency [27]. In the same study, the coumarins mammea A/BA and mammea C/OA also showed inhibitory activity against the proton pump, although with weaker effects (IC_{50} values of roughly 110 μM and 638 μM). The number and position of hydroxyl groups strongly influenced activity, underscoring the sensitivity of the pump to structural variations within these natural-product scaffolds. Although these compounds differ from the marine-derived molecules examined here, their reported activity supports the broader relevance of coumarin and xanthene frameworks in modulating gastric acid secretion. This provides a useful reference point when interpreting the docking results obtained for the marine metabolites.

The top-scoring compounds in our study shared several physicochemical features: moderate molecular size, balanced polarity and lipophilicity, and a relatively rigid framework. These properties are broadly consistent with those of many GPCR-active small molecules, which supports their potential to engage the H_2 receptor. Structural conservation within GPCR binding pockets, particularly among closely related receptor families, limits the chemical space available for achieving high selectivity. Ligands optimized for interactions with conserved residues may therefore retain

affinity across multiple GPCR subtypes, increasing the potential for off-target binding [75].

At the same time, the coumarin- and xanthene-based structures explored here occupy a region of chemical space distinct from currently used synthetic antagonists or P-CABs, offering different substitution patterns and oxygen-rich motifs that may interact with the H_2 receptor and proton pump in ways not accessible to existing drug classes. Taken together, these characteristics make them reasonable starting points for further chemical refinement.

Comparison of the docking interaction patterns with the DFT descriptors reveals qualitative rather than quantitative relationships. Compound **150**, which exhibits the smallest HOMO–LUMO gap together with the highest softness and electrophilicity, consistently adopts binding modes driven by complementary hydrophobic and π-mediated contacts supported by well-positioned polar anchors. In the H_2 receptor, stabilization involves π-type interactions and electrostatic complementarity with Asp98, whereas in the gastric proton pump the ligand engages a compact polar network involving Cys120, Gln127, Asn138 and Ala335, together with aromatic stabilization from Tyr799 and hydrophobic packing. This interaction profile is consistent with greater electronic adaptability and may contribute to the favorable docking scores observed for compound **150** against both targets, including its stronger predicted affinities relative to famotidine and soraprazan.

In contrast, compounds **1** and **5** display wider HOMO–LUMO gaps and lower electrophilicity, consistent with greater electronic stability and more localized interaction networks dominated by hydrogen bonding and steric or aromatic contacts. Although compound **5** shows the highest dipole moment, its binding appears largely shape-driven rather than strongly electrostatically optimized. Overall, these qualitative trends suggest that electronic flexibility may support adaptable binding across different protein environments.

ADME analysis showed that the selected ligands had generally favorable Caco-2 permeability (> −4.840 log cm/s) and low likelihood of inhibiting P-gp (0.009–0.369), although compounds **1** and **5** were predicted to be P-gp substrates (0.979 and 0.826, respectively), which may reduce their intracellular concentrations. Predicted intestinal absorption was high across the set of compounds (0.001–0.009), indicating good oral

uptake. All compounds showed low BBB penetration (0.001–0.292), which is an advantage for non-CNS targets, and exhibited markedly higher plasma protein binding (91–98%) than famotidine or soraprazan. The predicted CYP inhibition patterns suggest that selected candidates may interact with major metabolic enzymes such as CYP2C19 and CYP3A4. Compounds **1** and **5** displayed somewhat lower inhibition probabilities (0.019-0.630) compared to compound **150** (0.925–0.999). Predicted hERG inhibition was low for all molecules (0.078–0.281), indicating a limited cardiotoxicity risk. Overall, the candidates show encouraging pharmacokinetic features, but their high plasma-protein binding and CYP interaction profiles indicate areas where optimization will likely be required to improve exposure and minimize drug–drug interaction risk.

CONCLUSION

Our *in silico* results indicate that several of the marine-derived coumarin and xanthene compounds identified here appear suitable for further investigation as possible modulators of gastric acid secretion. Leptosphaerolide (compound **150**) in particular showed favorable predicted interactions with both the H_2 receptor and the proton pump, along with acceptable drug-likeness features. Penicixanthenes E and B (compounds **1** and **5**) also showed promising properties as H_2-receptor candidates. The calculated DFT parameters highlight distinct electronic profiles among the compounds and offer qualitative context for interpreting the observed docking trends. In conclusion, the combined use of molecular docking, virtual screening, and drug-likeness/ADMET analyses offers a practical framework for the early identification and prioritization of promising lead compounds, which may be further examined using molecular dynamics simulations. Overall, our findings provide a basis for continued exploration of these scaffolds and may support the development of acid-suppressive compounds with improved activity. Future studies should focus on the synthesis of prioritized candidates, *in vitro* binding and enzyme assays, and evaluation in gastric cell lines or *ex vivo* tissue models to confirm their inhibitory potential and biological relevance.

ACKNOWLEDGMENTS

This work was supported by the grant received from the Ministry of Science, Higher Education, and Youth of Sarajevo Canton, under the agreement number 27-02-35-37080-14/23 from 14. 9. 2023.

Conflicts of interest: Authors declare no conflicts of interest.

Funding: This research received no specific grant from any funding agency in the public, commercial, or not-for-profit sectors.

Data availability: The datasets generated during and/or analyzed during the current study are available from the corresponding author on reasonable request.

Submitted: December 2, 2025

Accepted: January 27, 2026

Published online: January 28, 2026

REFERENCES

1.Feldman M, Friedman LS, Brandt LJ, editors. *Sleisenger and Fordtran's Gastrointestinal and Liver Disease: Pathophysiology, Diagnosis, Management*. 11th ed. 2 vols. Philadelphia: Elsevier; 2020.

2.Katz PO, Dunbar KB, Schnoll-Sussman FH, Greer KB, Yadlapati R, Spechler SJ. ACG clinical guideline for the diagnosis and management of gastroesophageal reflux disease. *Am J Gastroenterol.* 2022;117(1):27–56. https://doi.org/10.14309/ajg.0000000000001538

3.Herndiana Y. Functional food in relation to gastroesophageal reflux disease (GERD). *Nutrients.* 2023;15(16):3583. https://doi.org/10.3390/nu15163583

4.Pesce M, Cargiolli M, Cassarano S, Polese B, De Conno B, Aurino L, et al. Diet and functional dyspepsia: clinical correlates and therapeutic perspectives. *World J Gastroenterol.* 2020;26(5):456–465. https://doi.org/10.3748/wjg.v26.i5.456

5.Rang HP, Dale MM, Ritter JM, Flower RJ, Henderson G. *Rang & Dale's Pharmacology*. 9th ed. Elsevier; 2020.

6.Tricco AC, Holbrook AM. Histamine H2 receptor antagonists for decreasing gastrointestinal harms in adults using acetylsalicylic acid: systematic review and meta-analysis. *Open Med.* 2012;6(3):e109–17.

7.McRorie JW Jr. Rapid development of tachyphylaxis with repeat dosing of H_2-receptor antagonists. *Ther Adv Gastroenterol.* 2014;5(2):57–62. https://doi.org/10.4292/wjgpt.v5.i2.57

8.Aldawsari FS, Alshehry YM, Alghamdi TS. N-nitrosodimethylamine (NDMA) contamination of ranitidine products: a review of recent findings. *Saudi Pharm J.* 2021;29(1):39–45. https://doi.org/10.38212/2224-6614.1133

9.Ketchem CJ, Lynch KL. Potassium-competitive acid blockers and proton pump inhibitors: the dynamic duo of acid blockers. *Gastroenterol Hepatol (N Y).* 2024;20(12):733–738.

10.Mori H, Suzuki H. Role of acid suppression in acid-related diseases: proton pump inhibitor and potassium-competitive acid blocker. *J Neurogastroenterol Motil.* 2019;25(1):6–14.
https://doi.org/10.5056/jnm18139

11.Tariq R, Singh S, Gupta A, Pardi DS, Khanna S. Association of gastric acid suppression with recurrent *Clostridium difficile* infection: systematic review and meta-analysis. *JAMA Intern Med.* 2017;177(6):784–791.
https://doi.org/10.1001/jamainternmed.2017.0212

12.Klatte DCF, Gasparini A, Xu H, de Deco P, Trevisan M, Johansson ALV, et al. Proton pump inhibitors and risk of chronic kidney disease: a systematic review and meta-analysis. *Gastroenterology.* 2017;153(3):702–710.
https://doi.org/10.1053/j.gastro.2017.05.046

13.Ochoa D, Román M, Cabaleiro T, Saiz-Rodríguez M, Mejía G, Abad-Santos F. Effect of food on the pharmacokinetics of omeprazole, pantoprazole and rabeprazole. *BMC Pharmacol Toxicol.* 2020;21:16.
https://doi.org/10.1186/s40360-020-00433-2

14.Antequera CM, Orleck K, Jacob R, Kenneally A, Wright WL. Potassium-competitive acid blockers: rethinking acid suppression for gastroesophageal reflux disease and *Helicobacter pylori*. *Postgrad Med.* 2024;136(2):131–140.
https://doi.org/10.1080/00325481.2024.2320081

15.Annunziata F, Pinna C, Dallavalle S, Tamborini L, Pinto A. An overview of coumarin as a versatile and readily accessible scaffold with broad-ranging biological activities. *Int J Mol Sci.* 2020;21(13):4618.
https://doi.org/10.3390/ijms21134618

16.Gomes SA, Brandão P, Garcia Fernandes CS, Ramos Pinto Correia da Silva M, Emília DSPDS, de Magalhães Pinto M. Drug-like properties and ADME of xanthone

derivatives: the antechamber of clinical trials. *Curr Med Chem.* 2016;23(32):3654–3686.
https://doi.org/10.2174/0929867323666160425113058

17.Bouhaoui A, Eddahmi M, Dib M, Khouili M, Aires A, Catto M, et al. Synthesis and biological properties of coumarin derivatives: a review. *ChemistrySelect.* 2021;6(24):5848–5870.
https://doi.org/10.1002/slct.202101346

18.Maia M, Resende DI, Duraes F, Pinto MM, Sousa E. Xanthenes in medicinal chemistry—synthetic strategies and biological activities. *Eur J Med Chem.* 2021;210:113085.
https://doi.org/10.1016/j.ejmech.2020.113085

19.Gallorini M, Carradori S, Resende DISP, Saso L, Ricci A, Palmeira A, et al. Natural and synthetic xanthone derivatives counteract oxidative stress via Nrf2 modulation in inflamed human macrophages. *Int J Mol Sci.* 2022;23(21):13319.
https://doi.org/10.3390/ijms232113319

20.Bai M, Zheng CJ, Nong XH, Zhou XM, Luo YP, Chen GY. Four new insecticidal xanthene derivatives from the mangrove-derived fungus *Penicillium* sp. JY246. *Mar Drugs.* 2019;17(12):649.
https://doi.org/10.3390/md17120649

21.Cao GP, Xia JL, Zhao LY, Tang ZZ, Lin X, Liu YH, et al. Penicixanthene E, a new xanthene isolated from a mangrove-derived fungus *Penicillium* sp. *J Antibiot.* 2022;75(9):526–529.
https://doi.org/10.1038/s41429-022-00548-0

22.Song F, Lin R, Yang N, Jia J, Wei S, Han J, et al. Antibacterial secondary metabolites from marine-derived *Aspergillus* sp. IMCASMF180035. *Antibiotics.* 2021;10(4):377.
https://doi.org/10.3390/antibiotics10040377

23.Blunt JW, Carroll AR, Copp BR, Davis RA, Keyzers RA, Prinsep MR. Marine natural products. *Nat Prod Rep.* 2016;34(1):235–294.
https://doi.org/10.1039/C7NP00052A

24.Soares JX, Loureiro DR, Dias AL, Reis S, Pinto MM, Afonso CM. Bioactive marine xanthones: a review. *Mar Drugs.* 2022;20(1):58.
https://doi.org/10.3390/md20010058

25.Fernández-Peña L, João Matos M, López E. Recent advances in biologically active coumarins from marine sources: synthesis and evaluation. *Mar Drugs.* 2022;21(1):37.
https://doi.org/10.3390/md21010037

26.Veríssimo ACS, Pinto DCGA, Silva AMS. Marine-derived xanthones from 2010 to 2021: isolation, biosynthesis, and biological activities. *Mar Drugs.* 2022;20(6):347.
https://doi.org/10.3390/md20060347

27.Reyes-Chilpa R, Baggio CH, Alavez-Solano D, Estrada-Muñiz E, Kauffman FC, Sanchez RI, et al. Inhibition of gastric H^+,K^+-ATPase activity by flavonoids, coumarins and xanthones isolated from Mexican medicinal plants. *J Ethnopharmacol.* 2006;105(1–2):167–172.
https://doi.org/10.1016/j.jep.2005.10.014

28.Shahzadi K, Bukhari SM, Zaidi A, Wani TA, Jan MS, Zargar S, et al. Novel coumarin derivatives as potential urease inhibitors for kidney stone prevention and anti-ulcer therapy: from synthesis to in vivo evaluation. *Pharmaceuticals (Basel).* 2023;16(11):1552.
https://doi.org/10.3390/ph16111552

29.Padole SS, Asnani AJ, Chaple DR, Katre SG. A review of approaches in computer-aided drug design in drug discovery. *GSC Biol Pharm Sci.* 2022;19(2):075–083.
https://doi.org/10.30574/gscbps.2022.19.2.0161

30.Pei Z. Computer-aided drug discovery: from traditional simulation methods to language models and quantum computing. *Cell Rep Phys Sci.* 2024;5:102334.
https://doi.org/10.1016/j.xcrp.2024.102334

31.Agu PC, Afiukwa CA, Orji OU, Ezeh EM, Ofoke IH, Ogbu CO, et al. Molecular docking as a tool for the discovery of molecular targets of nutraceuticals in disease management. *Sci Rep.* 2023;13(1):13398.
https://doi.org/10.1038/s41598-023-40160-2

32.Bickerton GR, Paolini GV, Besnard J, Muresan S, Hopkins AL. Quantifying the chemical beauty of drugs. *Nat Chem.* 2012;4(2):90–98.
https://doi.org/10.1038/nchem.1243

33.Vazquez-Rodriguez S, Matos MJ, Borges F, Uriarte E, Santana L. Bioactive coumarins from marine sources: origin, structural features and pharmacological properties. *Curr Top Med Chem.* 2015;15(17):1755–1766.
https://doi.org/10.2174/1568026615666150427125916

34.Guerriero A, D'Ambrosio M, Cuomo V, Pietra F. A novel, degraded polyketidic lactone, leptosphaerolide, and its likely diketone precursor, leptosphaerodione. Isolation from cultures of the marine ascomycete *Leptosphaeria oraemaris* (Linder). *Helv Chim Acta.* 1991;74(7):1445–1450.
https://doi.org/10.1002/hlca.19910740707

35.Chakraborty K, Antony T, Joy M. Prospective natural anti-inflammatory drimanes attenuating pro-inflammatory 5-lipoxygenase from marine macroalga *Gracilaria salicornia*. *Algal Res.* 2019;40:101472.
https://doi.org/10.1016/j.algal.2019.101472

36.Eltamany EE, Abdelmohsen UR, Ibrahim AK, Hassanean HA, Hentschel U, Ahmed SA. New antibacterial xanthone from the marine sponge-derived *Micrococcus* sp. EG45. *Bioorg Med Chem Lett.* 2014;24(21):4939–4942.
https://doi.org/10.1016/j.bmcl.2014.09.040

37.Fredimoses M, Zhou X, Ai W, Tian X, Yang B, Lin X, et al. Emerixanthone E, a new xanthone derivative from deep-sea fungus *Emericella* sp. SCSIO 05240. *Nat Prod Res.* 2019;33(14):2088–2094.
https://doi.org/10.1080/14786419.2018.1487966

38.He KY, Zhang C, Duan YR, Huang GL, Yang CY, Lu XR, et al. New chlorinated xanthone and anthraquinone produced by a mangrove-derived fungus *Penicillium citrinum* HL-5126. *J Antibiot.* 2017;70(7):823–827.
https://doi.org/10.1038/ja.2017.52

39.Hou JR, Wang YH, Zhong YN, Che TT, Hu Y, Bao J, et al. Protective effect of flavonoids from a deep-sea-derived *Arthrinium* sp. against ox-LDL-induced oxidative injury through activating AKT/Nrf2/HO-1 pathway in vascular endothelial cells. *Mar Drugs.* 2021;19(12):712.
https://doi.org/10.3390/md19120712

40.Kang HH, Zhang HB, Zhong MJ, Ma LY, Liu DS, Liu WZ, et al. Potential antiviral xanthones from a coastal saline soil fungus *Aspergillus iizukae*. *Mar Drugs.* 2018;16(11):449.
https://doi.org/10.3390/md16110449

41.Kong F, Carter GT. Remisporine B, a novel dimeric chromenone derived from spontaneous Diels-Alder reaction of remisporine A. *Tetrahedron Lett.* 2003;44(15):3119–3122.
https://doi.org/10.1016/S0040-4039(03)00518-5

42.Li HL, Li XM, Liu H, Meng LH, Wang BG. Two new diphenylketones and a new xanthone from *Talaromyces islandicus* EN-501, an endophytic fungus. *Mar Drugs.* 2016;14(12):223.
https://doi.org/10.3390/md14120223

43.Li X, Li XM, Wang BG. Structural revision of wentiquinone C and related congeners from anthraquinones to xanthones using chemical derivatization and NMR analysis. *Mar Drugs.* 2018;17(1):8.
https://doi.org/10.3390/md17010008

44.Liu FA, Lin X, Zhou X, Chen M, Huang X, Yang B, et al. Xanthones and quinolones derivatives produced by the deep-sea-derived fungus *Penicillium* sp. SCSIO Ind16F01. *Molecules.* 2017;22(12):1999.
https://doi.org/10.3390/molecules22121999

45.Ngan NT, Quang TH, Kim KW, Kim HJ, Sohn JH, Kang DG, et al. Anti-inflammatory effects of secondary metabolites from marine-derived *Penicillium* sp. strain SF-5629. *Arch Pharm Res.* 2017;40:328–337.
https://doi.org/10.1007/s12272-017-0890-5

46.Pan JH, Deng JJ, Chen YG, Gao JP, Lin YC, She ZG, et al. New lactone and xanthone derivatives produced by a mangrove endophytic fungus *Phoma* sp. SK3RW1M. *Helv Chim Acta.* 2010;93(7):1369–1374.
https://doi.org/10.1002/hlca.200900396

47.Resende DI, Almeida JR, Pereira S, Campos A, Lemos A, Plowman JE, et al. From natural xanthones to synthetic C-1 aminated 3,4-dioxygenated xanthones as optimized antifouling agents. *Mar Drugs.* 2021;19(11):638.
https://doi.org/10.3390/md19110638

48.Shao C, Wang C, Wei M, Gu Y, Xia X, She Z, et al. Two new xanthone derivatives from the marine fungus *Penicillium* sp. (ZZF 32#). *Magn Reson Chem.* 2008;46(11):1066–1069.
https://doi.org/10.1002/mrc.2293

49.Wang CN, Lu HM, Gao CH, Guo L, Zhan ZY, Wang JJ, et al. Cytotoxic benzopyranone and xanthone derivatives from coral symbiotic fungus *Cladosporium halotolerans* GXIMD 02502. *Nat Prod Res.* 2021;35(24):5596–5603.
https://doi.org/10.1080/14786419.2020.1799363

50.Wang HJ, Gloer JB, Scott JA, Malloch D. Coniochaetones A and B: new antifungal benzopyranones from *Coniochaeta saccardoi*. *Tetrahedron Lett.* 1995;36(33):5847–5850.
https://doi.org/10.1016/0040-4039(95)01174-G

51.Wang J, Ding W, Wang R, Du Y, Liu H, Kong X, et al. Identification and bioactivity of compounds from mangrove endophytic fungus *Alternaria* sp. *Mar Drugs.* 2015;13(7):4492–4504.
https://doi.org/10.3390/md13074492

52.Wang P, Luo YF, Zhang M, Dai JG, Wang WJ, Wu J. Three xanthone dimers from Thai mangrove endophytic fungus *Phomopsis* sp. xy21. *J Asian Nat Prod Res.* 2018;20(3):217–226.
https://doi.org/10.1080/10286020.2017.1333497

53.Wang X, Mao ZG, Song BB, Chen CH, Xiao WW, Hu B, et al. Structures and bioactivities of metabolites from mangrove-derived fungi in the South China Sea. *Mar Drugs.* 2013;11(10):3601–3616.
https://doi.org/10.3390/md11103601

54.Wu G, Yu G, Kurtán T, Mándi A, Peng J, Mo X, et al. Versixanthones A–F, cytotoxic xanthone-chromanone dimers from marine fungus *Aspergillus versicolor* HDN1009. *J Nat Prod.* 2015;78(11):2691–2698.
https://doi.org/10.1021/acs.jnatprod.5b00636

55.Xia MW, Cui CB, Li CW, Wu CJ, Peng JX, Li DH. Rare chromones from marine-derived *Penicillium purpurogenum* G59. *Mar Drugs.* 2015;13(8):5219–5236.
https://doi.org/10.3390/md13085219

56.Yu G, Wu G, Sun Z, Zhang X, Che Q, Gu Q, et al. Cytotoxic tetrahydroxanthone dimers from mangrove-associated *Aspergillus versicolor* HDN1009. *Mar Drugs.* 2018;16(9):335.
https://doi.org/10.3390/md16090335

57.Zhen X, Gong T, Wen YH, Yan DJ, Chen JJ, Zhu P. Chrysoxanthones A–C: three new xanthone-chromanone heterodimers from sponge-associated *Penicillium chrysogenum* HLS111. *Mar Drugs.* 2018;16(10):357.
https://doi.org/10.3390/md16100357

58.Zhu A, Zhang XW, Zhang M, Li W, Ma ZY, Zhu HJ, et al. Aspergixanthones I–K, new anti-*Vibrio* prenylxanthones from marine-derived *Aspergillus* sp. ZA-01. *Mar Drugs.* 2018;16(9):312.
https://doi.org/10.3390/md16090312

59.Krieger E, Vriend G. YASARA View—molecular graphics for all devices—from smartphones to workstations. *Bioinformatics.* 2014;30(20):2981–2982. https://doi.org/10.1093/bioinformatics/btu426

60.Krieger E, Vriend G. New ways to boost molecular dynamics simulations. *J Comput Chem.* 2015;36(13):996–1007. https://doi.org/10.1002/jcc.23899

61.Maier JA, Martinez C, Kasavajhala K, Wickstrom L, Hauser KE, Simmerling C. ff14SB: improving the accuracy of protein side chain and backbone parameters. *J Chem Theory Comput.* 2015;11(8):3696–3713. https://doi.org/10.1021/acs.jctc.5b00255

62.Chen VB, Arendall WB, Headd JJ, Keedy DA, Immormino RM, Kapral GJ, et al. MolProbity: all-atom structure validation for macromolecular crystallography. *Acta Crystallogr D Biol Crystallogr.* 2010;66(1):12–21. https://doi.org/10.1107/S0907444909042073

63.Lovell SC, Davis IW, Arendall III WB, De Bakker PI, Word JM, Prisant MG, et al. Structure validation by Cα geometry: ϕ, ψ and Cβ deviation. *Proteins.* 2003;50(3):437–450. https://doi.org/10.1002/prot.10286

64.Morris GM, Huey R, Lindstrom W, Sanner MF, Belew RK, Goodsell DS, et al. AutoDock4 and AutoDockTools4: automated docking with selective receptor flexibility. *J Comput Chem.* 2009;30(16):2785–2791. https://doi.org/10.1002/jcc.21256

65.Bento AP, Hersey A, Félix E, Landrum G, Gaulton A, Atkinson F, et al. An open-source chemical structure curation pipeline using RDKit. *J Cheminform.* 2020;12(1):51. https://doi.org/10.1186/s13321-020-00456-1

66.Shao Y, Molnar LF, Jung Y, Kussmann J, Ochsenfeld C, Brown ST, et al. Advances in methods and algorithms in a modern quantum chemistry program

package. *Phys Chem Chem Phys.* 2006;8(27):3172–3191.
https://doi.org/10.1039/B517914A

67.Parr RG, Szentpály LV, Liu S. Electrophilicity index. *J Am Chem Soc.* 1999;121(9):1922–1924.
https://doi.org/10.1021/ja983494x

68.Xiong G, Wu Z, Yi J, Fu L, Yang Z, Hsieh C, et al. ADMETlab 2.0: an integrated online platform for accurate and comprehensive predictions of ADMET properties. *Nucleic Acids Res.* 2021;49(W1):W5–14.
https://doi.org/10.1093/nar/gkab255

69.Copeland RA. *Evaluation of Enzyme Inhibitors in Drug Discovery: A Guide for Medicinal Chemists and Pharmacologists*. 2nd ed. Hoboken (NJ): Wiley; 2013.
https://doi.org/10.1002/9781118540398

70.Leeson PD, Bento AP, Gaulton A, Hersey A, Manners EJ, Radoux CJ, et al. Target-based evaluation of "drug-like" properties and ligand efficiencies. *J Med Chem.* 2021;64(11):7210–7230.
https://doi.org/10.1021/acs.jmedchem.1c00416

71.Robertson MJ, Papasergi-Scott MM, He F, Seven AB, Meyerowitz JG, Panova O, et al. Structure determination of inactive-state GPCRs with a universal nanobody. *Nat Struct Mol Biol.* 2022;29(12):1188–1195.
https://doi.org/10.1038/s41594-022-00859-8

72.Tanaka S, Morita M, Yamagishi T, Madapally HV, Hayashida K, Khandelia H, et al. Structural basis for binding of potassium-competitive acid blockers to the gastric proton pump. *J Med Chem.* 2022;65(11):7843–7853.
https://doi.org/10.1021/acs.jmedchem.2c00338

73.Leowattana W, Leowattana T. Potassium-competitive acid blockers and gastroesophageal reflux disease. *World J Gastroenterol.* 2022;28(28):3608–3619.
https://doi.org/10.3748/wjg.v28.i28.3608

74.Nowak A, Kutyła M, Kaczmarek J, Jaroszuk-Ściseł J, Jędryczka M. Differences in the production of extracellular polymeric substances (EPS) and other metabolites of *Plenodomus* (*Leptosphaeria*) infecting winter oilseed rape (*Brassica napus* L.). *Metabolites.* 2023;13(6):759.
https://doi.org/10.3390/metabo13060759

75.Ballante F, Kooistra AJ, Kampen S, de Graaf C, Carlsson J. Structure-based virtual screening for ligands of G protein-coupled receptors: what can molecular docking do for you? *Pharmacol Rev.* 2021;73(4):1698–1736.
https://doi.org/10.1124/pharmrev.120.000246

TABLES AND FIGURES WITH LEGENDS

Table 1. Docking and drug-likeness parameters of ligands evaluated against the H2 receptor and proton pump, exhibiting a QED greater than 0.67

	1 (H_2 receptor)	**5** (H_2 receptor)	**150** (H_2 receptor)	**150** (proton pump)
Binding energy [kcal/mol]	-7.49	-7.32	-7.78	-8.57
Dissociation constant [µM]	3.234	4.309	1.982	0.523
Ligand efficiency [kcal/(mol*Atom)]	0.375	0.293	0.338	0.373
MW [g/mol]	272.11	342.15	314.12	
logP	2.31	4.09	3.73	
HBD	1	3	1	
HBA	4	5	5	
TPSA [Å^2]	55.76	87	68.9	
RotB	0	5	4	
Arom	1	2	2	
Alerts	no	aryl carbonyl type motif	benzopyranone/coumarin-like substructure	
QED	0.787	0.713	0.871	
PAINS	no	no	no	

Abbreviations: MW: Molecular weight; logP: Lipophilicity; HBD: Hydrogen bond donors; HBA: Hydrogen bond acceptors; TPSA: Topological polar surface area; RotB: Rotatable bonds; Arom: Aromatic rings; QED: Quantitative estimate of drug-likeness; PAINS: Pan-Assay Interference Compounds substructures.

Table 2. Calculated quantum chemical parameters for compounds 1, 5, and 150

Quantum chemical parameters	1	5	150
Energy (au)	-920.226	-1151.484	-1072.842
E_{HOMO} (eV)	-5.87	-5.62	-5.29
E_{LUMO} (eV)	-1.31	-0.62	-1.74
ΔE (eV)	4.56	5.00	3.55
η (eV)	2.28	2.50	1.78
μ (eV)	-3.59	-3.12	-3.52
ω (eV)	2.83	1.95	3.48
S (eV^{-1})	0.22	0.20	0.28
Dipole moment (D)	2.17	4.14	3.24

Table 3. ADME parameters of optimal candidates selected based on binding affinity and drug-likeness metrics

Ligand	Caco-2 (log cm/s)	P-gp I	P-gp S	HIA	BBB	PPB	CYP 2C19	CYP 2D6	CYP 3A4	hERG
1	-4.761	0.369	0.979	<0.001	0.292	90.957	0.999	0.001	0.119	0.078
5	-4.840	0.311	0.826	0.009	0.045	95.416	0.630	0.784	0.472	0.098
150	-4.721	0.009	0.002	0.009	<0.001	98.343	0.999	0.959	0.925	0.281

Famotidine	-6.142	<0.001	1.000	0.073	<0.001	10.397	<0.001	<0.001	<0.001	0.281
Sorapazan	-5.352	0.082	0.215	<0.001	0.993	83.806	<0.001	0.002	0.009	0.124

Caco-2 permeability is expressed as log cm/s, with a proper Caco-2 permeability threshold set at > −5.15 log cm/s. The PPB (protein binding percentage) result is represented as a percentage, where a value of **<** 90% indicates that a sufficient amount of the drug remains unbound and is free to reach its target and traverse biological membranes. BBB penetration is also expressed as log cm/s, with logBBB > −1 categorized as BBB+ and logBBB ≤ −1 categorized as BBB−. The output value reflects the probability of a compound being classified as BBB+, ranging from 0 to 1. For the interpretation of HIA, P-gp, CYPs, and hERG results, classification models yield probability values between 0 and 1. Values within the range of 0–0.3 indicate a low probability of negative events (indicating a favorable profile), while values between 0.3 and 0.7 represent moderate or uncertain probabilities. Values from 0.7 to 1 suggest a high probability of negative events, indicating potential issues.

Abbreviations: ADME: Absorption, distribution, metabolism, excretion; Caco-2: Caco-2 cell monolayer permeability assay; P-gp: P-glycoprotein; P-gp I: P-glycoprotein inhibition; P-gp S: P-glycoprotein substrate; HIA: Human intestinal absorption; BBB: Blood–brain barrier; PPB: Plasma protein binding; CYP: Cytochrome P450; hERG: Human Ether-à-go-go-Related Gene.

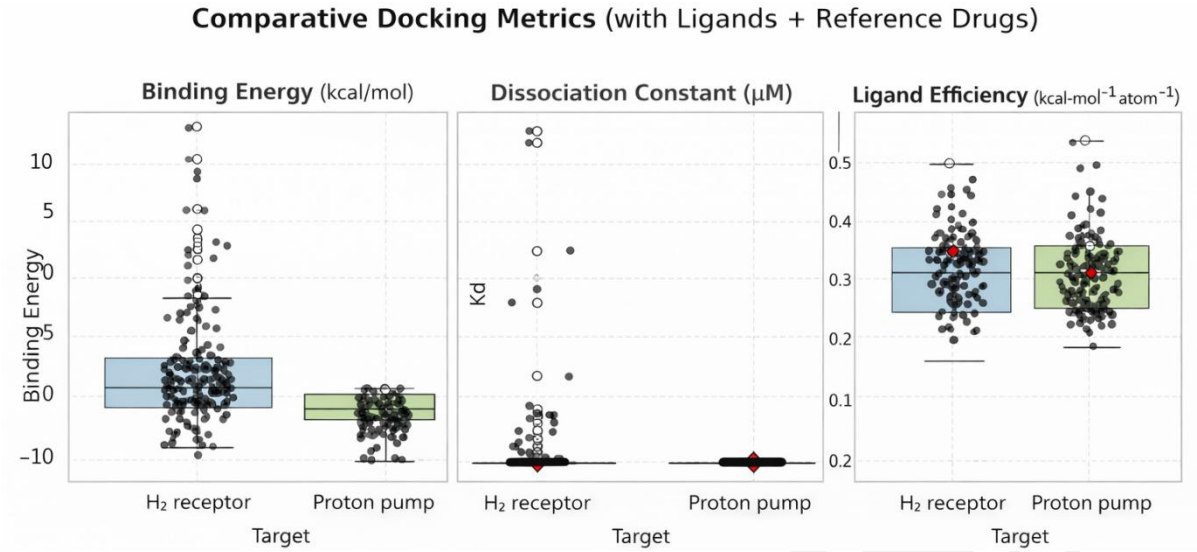

Figure 1. Comparative distribution of docking-derived metrics for the screened marine library against the histamine H_2 receptor and the gastric proton pump (H^+/K^+-ATPase). Box-and-whisker plots with overlaid individual data points summarize predicted binding free energies (ΔG, kcal/mol), dissociation constants (Kd, μM; estimated from ΔG), and ligand efficiencies (ΔG per heavy atom, kcal·mol^{-1}·atom^{-1}). Each point represents a single ligand from the screening set; boxes indicate the interquartile range with the median, whiskers extend to 1.5×IQR, and open circles denote outliers. Reference drugs are highlighted in red (famotidine for the H_2 receptor; soraprazan for the proton pump). **Abbreviations**: H_2: Histamine H_2; H^+/K^+-ATPase: Gastric H^+/K^+ adenosine triphosphatase (proton pump); ΔG: Binding free energy; Kd: Dissociation constant; IQR: Interquartile range.

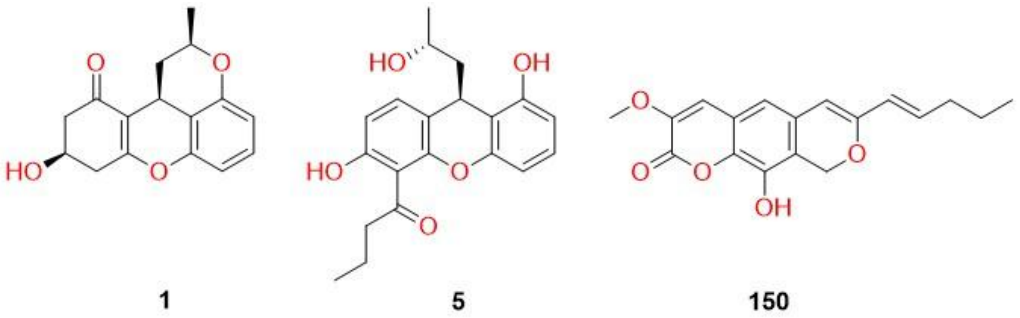

Figure 2. Chemical structures of the prioritized marine-derived hits (compounds 1, 5, and 150) selected after integrated docking and drug-likeness filtering. These three candidates outperformed famotidine in the histamine H_2 receptor docking screen and were the only molecules among the top binders that simultaneously satisfied Lipinski, Veber, and Egan criteria while maintaining QED > 0.67. Compounds 1 and 5 are xanthene derivatives, whereas compound 150 is a pyranocoumarin scaffold; compound 150 also emerged as the most stringent-filtered candidate in the gastric proton pump screen. **Abbreviations**: H_2: Histamine H_2; QED: Quantitative estimate of drug-likeness.

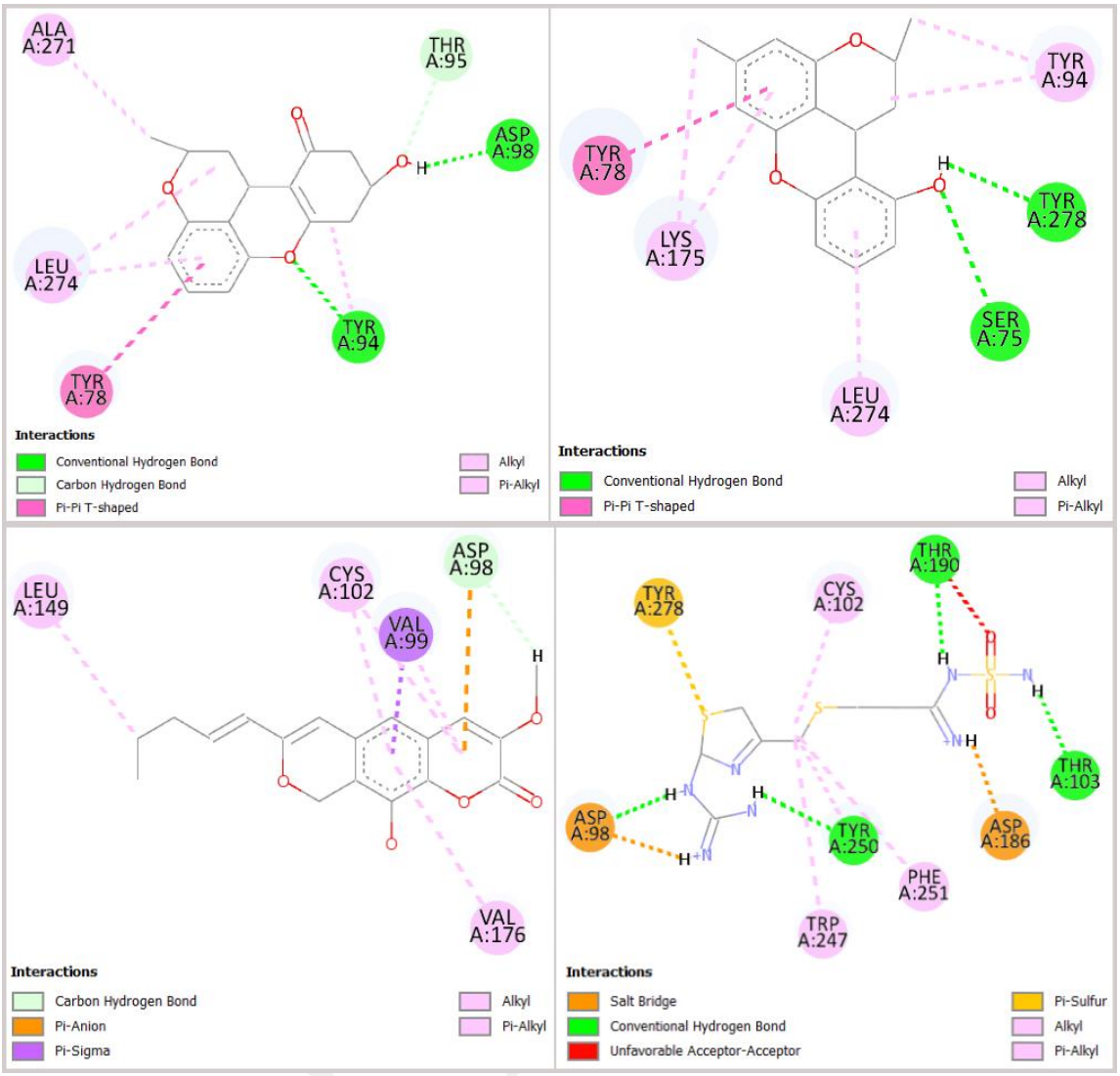

Figure 3. Protein–ligand interaction maps for prioritized marine hits docked to the histamine H_2 receptor. Two-dimensional interaction diagrams are shown for the best-ranked docking poses of compound 1 (top left), compound 5 (top right), compound 150 (bottom left), and the reference antagonist famotidine (bottom right). Compounds 1 and 5 (xanthene derivatives) display closely related binding patterns, sharing aromatic/hydrophobic contacts with Tyr78, Tyr94, and Leu274, but each is stabilized by a single dominant polar interaction (1: hydrogen bond to Asp98; 5: hydrogen bond to Tyr278). In contrast, compound 150 (pyranocoumarin scaffold) adopts a distinct pose characterized by π-mediated and hydrophobic stabilization with additional polar anchoring that overlaps with famotidine at Asp98 and Cys102. Interaction types are color-coded as indicated in each panel (e.g., hydrogen bonds, π–π/π-contacts, and hydrophobic contacts). **Abbreviations**: H_2: Histamine H_2; Asp:

Aspartate; Cys: Cysteine; Leu: Leucine; Lys: Lysine; Phe: Phenylalanine; Ser: Serine; Thr: Threonine; Trp: Tryptophan; Tyr: Tyrosine; Val: Valine.

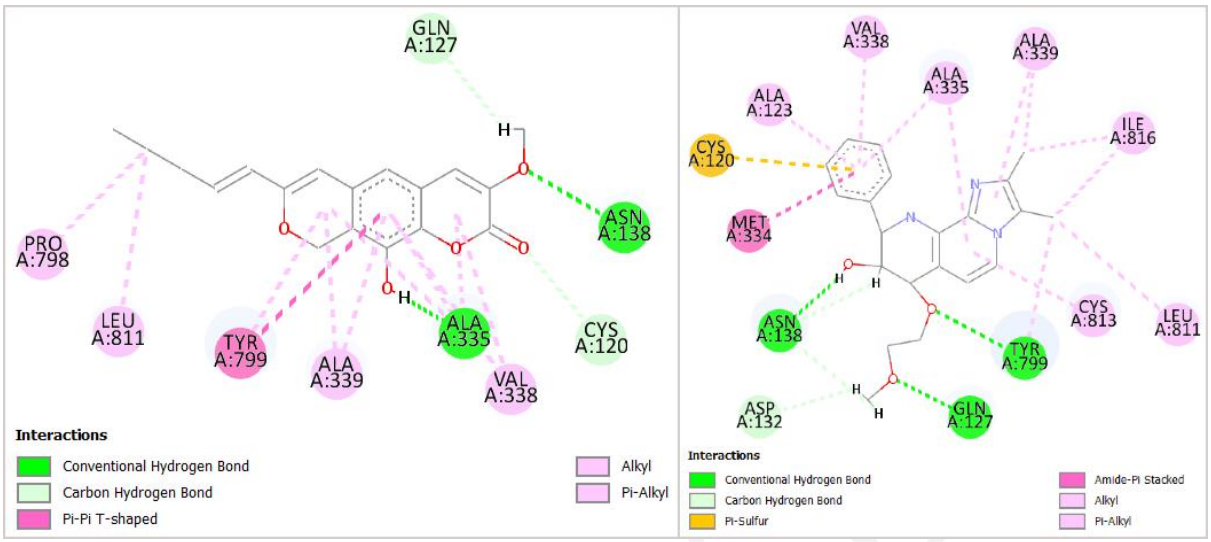

Figure 4. Comparative interaction maps of compound 150 and soraprazan docked to the gastric proton pump (H^+/K^+-ATPase). Two-dimensional (2D) protein–ligand interaction diagrams are shown for the best-ranked docking poses of compound 150 (left) and the reference potassium-competitive acid blocker soraprazan (right). Compound 150 reproduces a binding pattern closely matching soraprazan within the K^+-site pocket, sharing a conserved interaction network anchored by Cys120, Gln127, and Asn138, and reinforced by hydrophobic/π-mediated contacts with Ala335, Ala339, Val338, Tyr799, and Leu811. Overall, eight of the nine key residue contacts observed for compound 150 are also present in the soraprazan binding mode, supporting a highly overlapping pose consistent with competitive engagement of the proton-pump pocket. Interaction types are color-coded within each panel (e.g., hydrogen bonds, π-interactions, and hydrophobic contacts).
Abbreviations: H^+/K^+-ATPase: Gastric H^+/K^+ adenosine triphosphatase (proton pump); 2D: Two-dimensional; Ala: Alanine; Asn: Asparagine; Asp: Aspartate; Cys: Cysteine; Gln: Glutamine; Ile: Isoleucine; Leu: Leucine; Met: Methionine; Pro: Proline; Tyr: Tyrosine; Val: Valine.

SUPPLEMENTAL DATA

Supplemental data are available at the following links:

https://www.bjbms.org/ojs/index.php/bjbms/article/view/13660/4115

https://www.bjbms.org/ojs/index.php/bjbms/article/view/13660/4116